

Article

Direct Electrical Sensing of Iodine Gas by a Covalent Organic Framework-Based Sensor

Wanshuang Zhou¹, Chun Kang¹, Cong Yu¹ , Zhaojie Cui¹ and Xinbo Wang^{1,2,*}

¹ School of Environmental Science and Engineering, Shandong Key Laboratory of Environmental Processes and Health, Shandong University, No. 72 Binhai Road, Qingdao 266237, China

² Shenzhen Research Institute, Shandong University, Virtual University Park, Nanshan District, Shenzhen 518057, China

* Correspondence: wangxb@sdu.edu.cn

Abstract: Rapid and highly sensitive detection of iodine gaseous species is crucial as the first response in case of nuclear accidents and nuclear waste clean-up. A robust and user-friendly sensor-based technology that allows online monitoring is highly desirable. Herein, we report the success of using a covalent organic framework (AQ-COF)-based sensor for real-time iodine gas adsorption and detection by the electrochemical impedance spectroscopy (EIS) technique. The sensor exhibits a high sensitivity and a pronounced electrical response to trace amounts of iodine vapor. Gaseous iodine was readily detected with a significant change in resistance ($10^4 \times$) at 70 °C within 5 min exposure to air. Notably, the EIS response is quite chemoselective to iodine over other common species such as air, methanol, ethanol, and water, with a selectivity of 320, 14, 49, and 1030, respectively. A mechanical study shows that the adsorption of iodine can reduce the optical bandgap of the AQ-COF, causing the impedance to drop significantly. This study demonstrates how the adsorption enrichment effect of selective I₂ adsorption by a covalent organic framework can be leveraged to create a highly selective sensor for the direct online electrical detection of radioactive gaseous toxins.

Keywords: covalent organic frameworks; COFs; iodine vapor; sensor; direct sensing; electric impedance spectroscopy



Citation: Zhou, W.; Kang, C.; Yu, C.; Cui, Z.; Wang, X. Direct Electrical Sensing of Iodine Gas by a Covalent Organic Framework-Based Sensor. *Atmosphere* **2023**, *14*, 181. <https://doi.org/10.3390/atmos14010181>

Academic Editors: Xiaorong Gan, Baojun Liu, Jianlin Zhang and Gang Zhou

Received: 21 December 2022

Revised: 3 January 2023

Accepted: 11 January 2023

Published: 14 January 2023



Copyright: © 2023 by the authors. Licensee MDPI, Basel, Switzerland. This article is an open access article distributed under the terms and conditions of the Creative Commons Attribution (CC BY) license (<https://creativecommons.org/licenses/by/4.0/>).

1. Introduction

The highly sensitive detection of fission gas is of great importance for the protection of both animals and plants, particularly in the field of nuclear industry, as this field is always accompanied by the production of nuclear waste. Iodine radioisotopes (¹²⁹I and ¹³¹I) are the two major concerns linked to nuclear fission because of their volatile and radioactive nature [1–3]. In particular, while ¹³¹I has a short half-life (8 d) but strong negative activity in human metabolic processes, ¹²⁹I has an ultra-long half-life (1.57×10^7 y) [4–6]. What is more, iodine is easily volatilized to the atmosphere, causing ozone destruction in the stratosphere [7], and can accumulate in living organisms via gas inhalation or the food chain, resulting in thyroid diseases and cancer [8,9]. In the case of a nuclear accident or inadvertent environmental release of radioactive iodine vapour, remarkable efforts are being made to improve the detection technics for early warning and first responses [10–12]. Among which, electrochemical impedance spectroscopy (EIS), combining a highly selective material with electrical readout responses, has been a promising technic for direct electrical detection of iodine gas [13,14].

Covalent organic frameworks (COFs), a new type of crystalline porous material, have been attracting a significant interest in recent decades [15–17]. As a result of their excellent porosity, periodic framework, fine tunable structure, chemical/thermal stability, and host-guest interactions, COFs are a promising platform for broad applications, such as gas separation [18], catalysis [19,20], electrochemical energy storage [21,22], proton conduction [23], optical/electrical sensing [24,25], and other fields. COFs are conductive

to the transport of substances because of their highly regular, ordered pore structure and adjustable pore size, which can speed up the entire interaction between targeting analytes and sensing materials and so promote the effective detection of chemicals. At the same time, the stable covalent bonding allows COFs to retain their original structure under harsh conditions [26], providing an ideal platform for corrosive gas, e.g., I₂, adsorption and sensing [27–29]. However, COF-based chemical sensors have been reported but are mainly limited to the transduction mechanisms based on luminescence quenching or enhancement [30,31]. On the other hand, COF-based electrical sensors are relatively rare [32]. To our best knowledge, the use of COFs as a sensing material for EIS has not been explored.

In this work, we reported the synthesis of an anthraquinone-containing COF (AQ-COF) linked by β -keto amines with unique enol-keto tautomerism structure. The synthesized AQ-COF was used for the first time as a sensitive material for electrochemical sensing. High sensitivity towards iodine gas was demonstrated, with a resistance change over $10^4\times$ of the AQ-COF-based sensing film coated on the surface of the active area of Au-interdigitated electrodes (IDEs) within only 5 min at 70 °C. It is worth mentioning that AQ-COF exhibits a selective impedance change to iodine molecules at room temperature, without being affected by air, water vapor, methanol, or ethanol vapor. This study reveals a novel method for the fabrication of gas sensors based on COFs and provides a new perspective for the design of advanced gas sensors with high detection efficiency, sensitivity, and selectivity.

2. Materials and Methods

2.1. Materials

1,3,5-triformylphloroglucinol (TFP) was synthesized following a reported procedure [15]. A MilliQ System (Millipore, Inc., Billerica, MA, USA) was used to apply deionized water (DI) water. All other chemicals were obtained from Sinopharm (Shanghai, China) and used as received.

2.2. Characterization

Solid-state nuclear magnetic resonance spectroscopy (NMR) was performed on a Bruker NMR spectrometer (ADVANCE III 600). N₂ adsorption–desorption isotherms for the AQ-COF at 77 K were obtained by a physisorption instrument (BSD-PM2). Thermogravimetric analyses (TGA) were conducted on a Netzsch TG 209 F3 analyzer. The powder X-ray diffraction (PXRD) experiments were conducted on an X-ray diffractometer (Bruker D8 ADVANCE) equipped with a Cu K α radiation source, with scanning at rate of 1°/min from 2.5 to 40°. A BRUKER TENSOR 27 FT-IR spectrometer was used for Fourier transform infrared (FTIR) spectra. UV-Vis absorption spectra were acquired on a Shimadzu UV-2600i (Shimadzu, Tokyo, Japan) with a wavelength ranging from 200 to 800 nm, using BaSO₄ as the reference. X-ray photoelectron spectroscopy (XPS) was performed on a Thermo Scientific ESCALAB Xi+. The electrochemical impedance response was analyzed on a Corrtest CS 310M workstation. The highest input impedance of this workstation was 10¹² Ω . The frequency range of the alternating current was 100 kHz–10 mHz, and the perturbation amplitude was 50 mV. The experiments were conducted at room temperature with sensors placed on an alumina plate that was 5 mm thick. The Zview software version 3.1 (Scribner and Associates Inc., Southern Pines, NC, USA) was used to fit their impedance plots using equivalent circuits.

2.3. Synthesis of the AQ-COF

An amount of 0.9 mmol (189 mg) of TFP and 1.35 mmol (321.3 mg) of 2,6-diaminoanthraquinone (DAAQ) in a Pyrex tube were added to 9 mL of mesitylene and 1,4-dioxane (1:1 volume). After 10 min of sonication, the mixture formed a uniform solution, and then 1.5 mL of 6 M aqueous acetic acid was added to the mixture dropwise at room temperature. Degassing was carried out by three cycles of freeze–exhaust–thaw in a liquid nitrogen bath. The reaction tube was flame sealed and kept at 120 °C for 72 h. After cooling to room

temperature, the mixture was filtered and a red precipitate was obtained after extensive washing with acetone, methylene chloride, and ethanol. Then, Soxhlet was extracted with ethanol for one day. Finally, a maroon solid was obtained after drying under vacuum at 70 °C for 24 h.

2.4. Sensor Fabrication

The Au-interdigitated electrodes (IDEs) on an alumina substrate were supplied by Guangzhou Yuxin Sensor Technology Co., Ltd. (Guangzhou, China). The active area of the electrode was around 0.3 cm². Each electrode contained 10 pairs of gold lines with a width of 100 μm, at 100 μm apart from each other. Before use, the IDEs were pre-treated by soaking in methanol for 10 min and dried under a flow of N₂. The blank IDEs were measured and had impedances higher than $1.1 \times 10^{10} \Omega$ at 10 mHz. An amount of 10 mg of AQ-COF was dispersed in 1 mL methanol by sonication and then 10 μL was pipetted to the active area of IDE. After drying for 10 min on a heating plate, a thin film of AQ-COF was formed on the surface of the IDE. Before exposure to the analyte, the sensor was pre-dried in a drying oven at 70 °C for 30 min.

2.5. Iodine Gas Exposure

A 250 mL glass bottle with lip containing 200 mg iodine powder was heated to 70 °C in a constant temperature oven for 2 h to reach iodine vapor equilibrium. The sensor was then put into the vial and kept for different time intervals of 0.5, 1, and 5 min. After this, the sensor was immediately taken out from the vial and employed directly for EIS measurement without further processing. At least three runs of each experiment were completed.

2.6. Selectivity Test

Air, methanol, ethanol, and water were also investigated as possible chemical interfering species, in a similar way to iodine gas, but using another analyte instead of iodine. In order to produce saturated vapor pressure for other chemically disturbed species, 10 mL of methanol, ethanol, or water were put in 250 mL clean glass vials and held at room temperature for 2 h. After that, the sensors were each sealed for 5 min in vials and removed right away for EIS measurements.

3. Results and Discussion

3.1. Materials Synthesis and Characterization

The AQ-COF powder was synthesized by a solvothermal method, with slight modifications to a reported protocol [33]. The compounds 1,3,5-triformylphloroglucinol (TFP) and 2,6-diaminoan-thraquinone (DAAQ) were Schiff-condensed to synthesize AQ-COF with a solvent mixture of anhydrous 1,4-dioxane, mesitylene, and acetic acid (Figure S1).

The ¹³C solid-state NMR spectra (CP-MAS) were obtained and are depicted in Figure 1a. The characteristic signal peaks of keto at 181 ppm and an enol-imine carbon signal at 148 ppm suggest the successful synthesis of the AQ-COF framework dominated with the known enol-imine structure. The high crystallinity of AQ-COF was confirmed by powder XRD patterns (Figure 1b). AQ-COF shows intense diffraction peaks at $2\theta = 3.14, 5.90, 6.82, 12.72, 22.78,$ and 26.83° , which can be assigned to the (100), (110), (220), (101), (202), and (001) facets, respectively. The composition of the AQ-COF was further investigated by XPS analysis. As shown in Figure S2, two characteristic peaks in the O 1s high resolution spectra, i.e., the C=O of the keto-amine (531.23 eV) and the C-OH of the enol-imine (532.79 eV), were observed. Meanwhile, characteristic peaks at 399.26 eV, 400.24 eV, and 404.86 eV in the N 1s core level spectrum correspond to the C=N in the enol-imine, C-NH in the keto-amine, and π excitation, respectively [33–36]. These results suggest AQ-COF is in an equilibrium of both its keto-amine and enol-imine forms.

SEM imaging of the powder revealed a micro-sized fiber-like morphology, which self-assembled into nanoflowers (Figure S3). Thermogravimetric analyses (TGA) disclosed the high decomposition temperature of AQ-COF, of above 316 °C (Figure S4), indicating its

high thermostability. The porous nature of AQ-COF was measured by N_2 physisorption at the temperature of liquid nitrogen, and typical isotherms are depicted in Figure 1c. A typical I-type reversible isotherm was demonstrated, indicating that AQ-COF contains a large number of microporous structures. The specific surface area of pristine AQ-COF was calculated to be about $706 \text{ m}^2/\text{g}$ from the adsorption curve with the Brunauer–Emmett–Teller (BET) method, indicating the microporous nature of the material. Such a microporous architecture of AQ-COF contains open and interconnected voids for guest molecules, which is expected to improve its adsorption capacity and selectivity because of the high surface area and size sieving effect [10,37]. Indeed, in a static iodine adsorption experiment (Figure 1d), AQ-COF adsorbs iodine quickly once exposed to the iodine gas environment and quickly achieved equilibrium within 4 h. It is worth mentioning that the capacity of $470 \text{ mg}\cdot\text{g}^{-1}$ for AQ-COF is much higher than the capacity of Ln-MOF ($340 \text{ mg}\cdot\text{g}^{-1}$) [37]. In addition, the iodine adsorption properties of AQ-COF and other COF materials are compared in Table S1 [27,38–42].

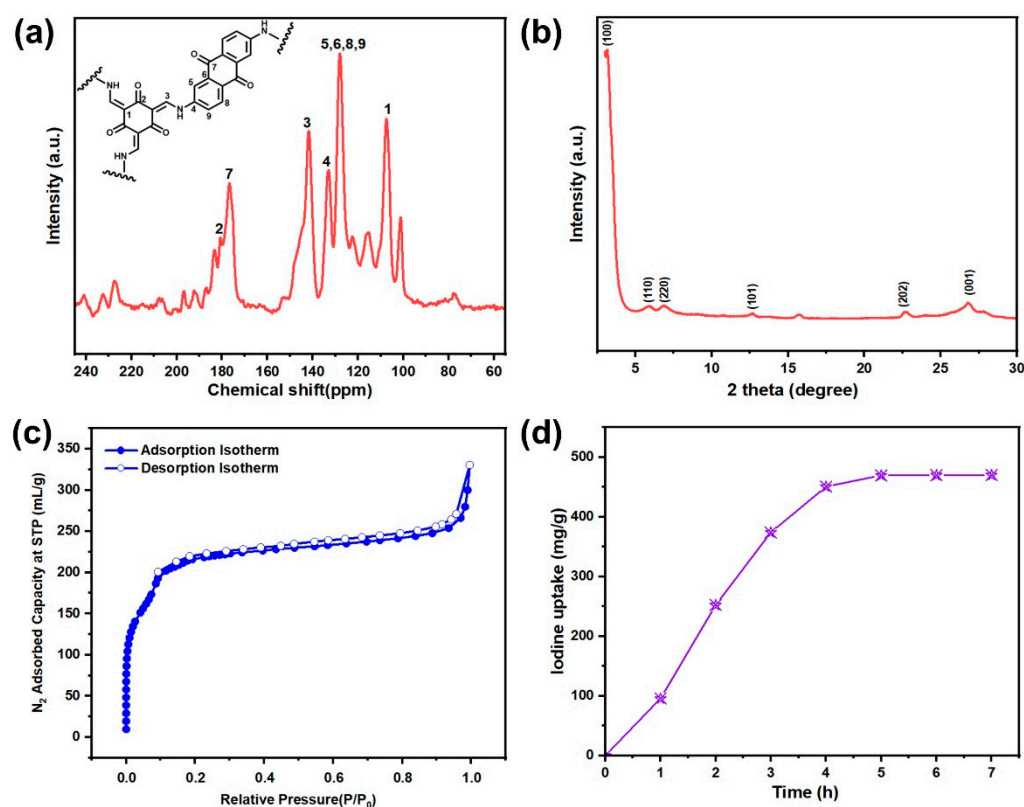


Figure 1. (a) ^{13}C solid-state NMR spectrum of the AQ-COF, (b) PXRD patterns of the AQ-COF, (c) N_2 physisorption isotherms for the AQ-COF at liquid nitrogen temperature, and (d) iodine uptake of the AQ-COF at 70°C .

3.2. Sensor Fabrication and the Iodine Vapor Impedance Sensing

The AQ-COF powders were well pipetted onto the active area of the IDE to form a sensing film layer as described in the experimental section, and the sensor was subsequently exposed to gaseous iodine at 70°C for different time intervals. The typical impedance spectra are presented as the impedance amplitude and phase spectrum in the frequency range of 10 mHz – 100 kHz (Figure 2a). The blank IDE displays a very high capacitive response, with the impedance, $|Z|$, increasing linearly to $>10^{10} \Omega$ with decreasing frequency from 100 kHz to 10 mHz . The phase angle was almost -90° for all the frequencies. Upon AQ-COF coating, neither the impedance nor the phase angle changed appreciably in the air, indicating the highly capacitive nature. After iodine exposure at 70°C for 5 min, however, the I_2 was adsorbed and the low-frequency impedance, $|Z|$, sharply leveled out to $10^7 \Omega$

below 10 Hz, three orders of magnitude lower than the pristine sample. Simultaneously, the phase angle significantly changed from -90° to 0° , indicating the electrical response had changed from capacitive to resistive.

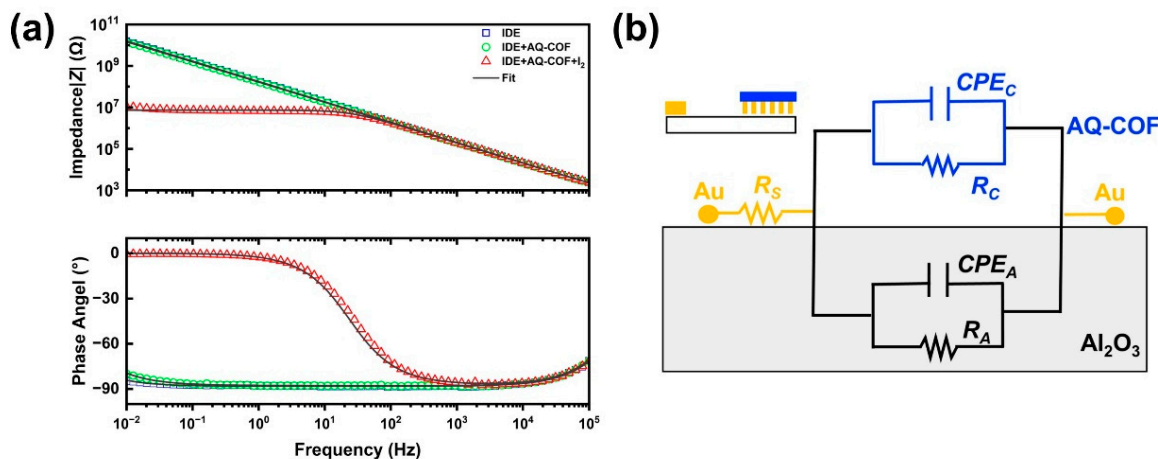


Figure 2. (a) Impedance and phase angle of pristine IDE and AQ-COF coated IDE under different conditions as a function of frequency. (b) A simplified equivalent circuit model of the electrical system.

To better quantify the electrochemical response and obtain additional information through the extraction of meta-variables, the Bode plots in Figure 2a were fitted and analyzed using Zview software, and a simplified equivalent circuit model was proposed to describe the impedance behavior of the system, as depicted in Figure 2b [11]. In the specified circuit, two parallel shunt resistance–capacitor (R/CPE) networks were connected in series with a series resistor, R_S . The series resistance, R_S , was usually $660 \pm 5 \Omega$ for each sensor, mainly due to the metal wire on the sensor. The R_A , CPE_A , R_C , and CPE_C are the resistance and capacitance of the alumina substrate and the resistance and capacitance of the AQ-COF coating, respectively. The CPE is a frequency-dependent constant phase element that describes the non-ideal behavior of the electrode due to the roughness and non-uniform surface [43]. To obtain the most consistent fitting results, the variables of R_S (669Ω), R_A ($\approx 2.3 \times 10^{11} \Omega$), and CPE_A (0.5 – 0.9 nF) were fixed by recording the values for the blank sensor and used for the subsequent analysis [11].

3.3. Time-Dependent Sensor Response

The sensitivity of the activated sensor was first evaluated by monitoring the impedance changes with varying exposure time to iodine vapor. The charge transfer resistance (R_C) is the most important circuit element because it is directly related to sensor accessibility and reflects the flow of charge into the electrode through the interface. The response of the AQ-COF-based sensor is defined as $(R_0 - R_C)/R_C$ to reflect the response intensity, where R_0 and R_C represent the original resistance and the change in resistance upon exposure to the analyte, respectively [44]. As shown in Figure 3, the pristine blank IDE showed a quite low response, with response values of 2.67, 3.97, and 49.28 after iodine exposure for 0.5, 1, and 5 min, respectively. Upon AQ-COF coating, but without iodine exposure, the response was constantly maintained at a low value of <0.6 with prolonged time. As expected, on the other hand, a significant increase in the gas response with increasing iodine exposure time was obtained for AQ-COF sensor, with values of 81.66, 162.49, and 3.14×10^4 , at the exposure times of 0.5, 1, and 5 min, respectively. The response (4 orders of magnitude change after 5 min exposure) is lower than the PIM-1 membrane-based iodine EIS sensor that we have reported earlier (7 orders of magnitude change) [11], but comparable with MOF-based EIS sensors [13,14]. It is worth mentioning that MOFs constructed with metal–organic coordination are inherently less stable than COFs which are covalently bonded, particularly in water stability. In addition, the responses of MOF-based EIS sensors are much slower

(30 min to several hours at 70 °C) than the AQ-COF sensors. A timely and high response are equally important for the first response in case of a nuclear accident.

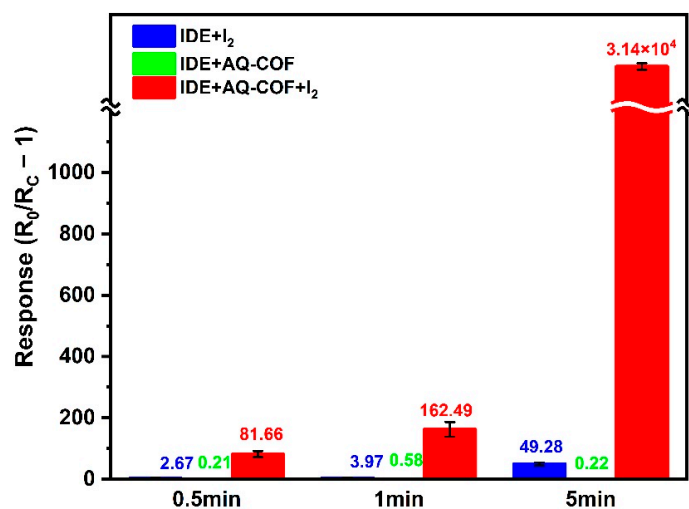


Figure 3. The response of the IDE sensors with or without AQ-COF coating at 70 °C as a function of time.

3.4. Selectivity

For application under real conditions, high chemical selectivity of the sensor is of great importance to give reliable output signals, since the real gas is always a complex mixture of many components. The selectivity of the AQ-COF sensor was investigated by comparing the resistance response against potentially interfering chemicals, including air, methanol, ethanol, and water. The selectivity, S , towards iodine to other species was defined as $S = \text{Response (I}_2\text{)}/\text{Response (chemically disturbed species)}$, and the results are shown in Figure 4. It was found that there were no appreciable resistance changes in the sensor to any of these chemicals. The resistance response values varied slightly and were all less than 15, which were far lower than the value obtained for iodine (211.36). The selectivity, S , values were calculated to be 319.23, 14.20, 48.97, and 1029.85 for air, methanol, ethanol, and water, respectively, indicating that the AQ-COF sensor had good selectivity and specificity towards iodine vapor. The water stability and low moisture response indicate that the material is promising for real applications.

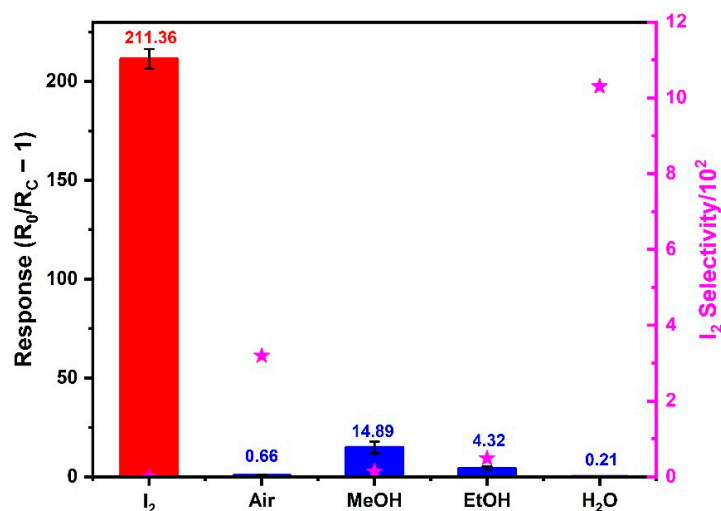


Figure 4. The gas response (histograms) and selectivity (stars) of AQ-COF-based IDE sensor towards various gaseous molecules.

3.5. Mechanism Study

In order to understand the electrochemical interaction mechanism between the iodine vapor and the AQ-COF/IDE, further experiments were carried out. Firstly, FT-IR measurements were conducted to investigate the structure changes of the AQ-COF after iodine exposure. As presented in Figure 5a, the FTIR spectra of AQ-COF before and after iodine doping are almost identical, indicating that no functional group changes occurred. However, the characteristic absorbances at 1252, 1564, and 1620 cm^{-1} , belonging to the C-N, C=C, and C=O bonds of β -ketoenamine, downshifted slightly to 1249 cm^{-1} , 1560 cm^{-1} , and 1614 cm^{-1} , respectively, indicating the existence of interactions between AQ-COF and iodine molecules. Then, solid-state UV-Vis spectroscopy was used to analyze the optical characteristics of AQ-COF before and after iodine loading. The optical bandgap of AQ-COF and the I_2 -laden AQ-COF were assessed by a Tauc plot (Figure 5b). An approximate extrapolation of the linear region of the transition map resulted in an optical bandgap (E_g) of 1.49 and 1.11 eV for AQ-COF before and after iodine exposure, respectively. The reduction in the optical bandgap by approximately 34% in the iodine-laden AQ-COF suggests new pathways for charge transfer had been created, causing a significant improvement in conductivity.

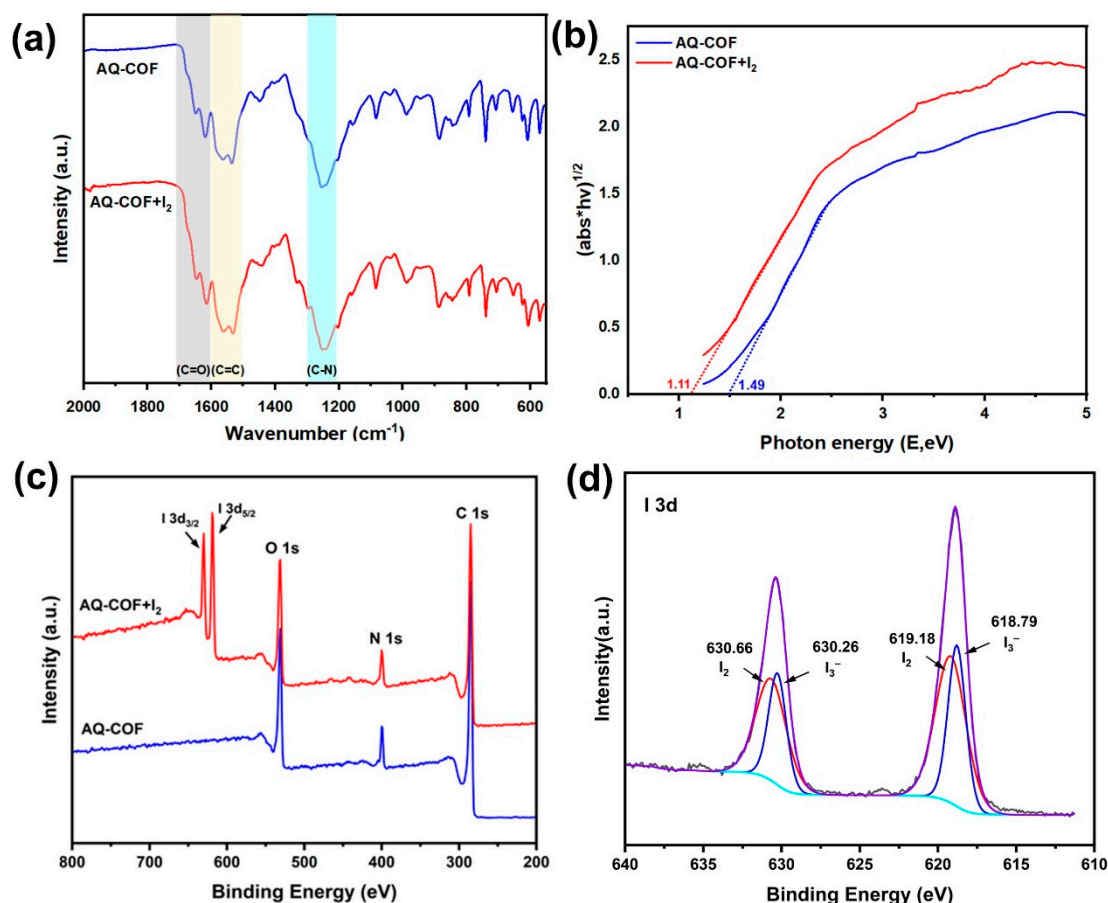


Figure 5. (a) FT-IR spectra of AQ-COF and I_2 vapor adsorbed AQ-COF. It contains C=O (grey), C=C (yellow) and C-N (blue) bands of vibration. (b) The optical band gap of AQ-COF and I_2 vapor adsorbed AQ-COF, (c) XPS survey spectra of AQ-COF and I_2 vapor adsorbed AQ-COF, and (d) XPS spectra of I_2 vapor adsorbed AQ-COF.

Thirdly, X-ray photoelectron spectroscopy (XPS) was performed to analyze the chemical composition and the chemical oxidation state of elements in the composite. The full spectrum of the XPS survey clearly presented peaks of C 1s, N 1s, and O 1s for pristine AQ-COF, while two new strong and sharp peaks, assigned to I 3d_{3/2} and I 3d_{5/2}, were

observed in the I 3d region for the I₂-laden AQ-COF (Figure 5c), indicating the adsorption of iodine on the surface of the framework. Deconvolution of the high resolution I 3d peaks resulted in two types of iodine, which are zero valence I₂ (binding energy centered at 630.66 eV and 619.18 eV) and polyiodide anions, I₃[−] (binding energy centered at 630.26 eV and 618.79 eV), similar to what was observed for I₂-laden PIM-1 [11]. Combining the above results, it can be concluded that it appears that charge transfer occurred in the π electrons of the conjugated framework and guest iodine molecules. The formation of the more conductive ion, I₃[−], may be responsible for the low resistance.

4. Conclusions

In summary, we demonstrated a COF-based gas sensing platform for direct electrical iodine vapor detection using the EIS technique in critical environments. The sensor exhibits an excellent I₂ sensing performance with a fast response and high sensitivity and selectivity. A high response factor of up to 10⁴ × was obtained within 5 min of exposure. On the other hand, the sensor is silent to other potentially interfering species such as air, water, methanol, and ethanol, with a chemical selectivity of up to 10³. Further optimization of the sensor fabrication process and the active layer geometry to minimize the COF thickness and maximize the sensing capacity towards trace iodine detection is ongoing. The success of this research not only provides an effective way to monitor iodine leakage, but also opens the prospect for the design of COF-based sensing devices in the future.

Supplementary Materials: The following supporting information can be downloaded at: <https://www.mdpi.com/article/10.3390/atmos14010181/s1>, Figure S1: Scheme illustration of the synthesis of AQ-COF; Figure S2: N1s (a,b) and O1s (c,d) spectra of AQ-COF before and after iodine adsorption. Figure S3: SEM image of AQ-COF. Figure S4: TG analysis of AQ-COF.

Author Contributions: Conceptualization, X.W. and W.Z.; methodology, W.Z.; software, W.Z.; validation, W.Z. and C.Y.; formal analysis, C.K.; investigation, W.Z.; resources, X.W. and W.Z.; data curation, W.Z.; writing—original draft preparation, W.Z.; writing—review and editing, X.W.; supervision, X.W. and Z.C.; funding acquisition, X.W. All authors have read and agreed to the published version of the manuscript.

Funding: This research was funded by the National Natural Science Foundation of China (22078174, 21908018), Guangdong Basic and Applied Basic Research Foundation (2022A1515011856), Shenzhen Science and Technology Program (JCYJ20220530141205012), Shandong University for QiLu Young Scholar Start-up Foundation, and with support from the State Key Laboratory of Fine Chemicals, Dalian University of Technology (KF 2114).

Institutional Review Board Statement: Not applicable.

Informed Consent Statement: Not applicable.

Data Availability Statement: Data are available in the SI or by contacting the authors.

Acknowledgments: We thank Haiyan Sui from the State Key Laboratory of Microbial Technology of Shandong University for her kind help in material characterizations. We also appreciate the FT-IR measurements by Min Zhang from Analytical Testing Center, School of Environmental Science and Engineering, Shandong University.

Conflicts of Interest: The authors declare no conflict of interest.

References

1. Guo, X.; Li, Y.; Zhang, M.; Cao, K.; Tian, Y.; Qi, Y.; Li, S.; Li, K.; Yu, X.; Ma, L. Colyliform Crystalline 2D Covalent Organic Frameworks (COFs) with Quasi-3D Topologies for Rapid I₂ Adsorption. *Angew. Chem. Int. Ed.* **2020**, *59*, 22697–22705. [[CrossRef](#)] [[PubMed](#)]
2. Ten Hoeve, J.E.; Jacobson, M.Z. Worldwide health effects of the Fukushima Daiichi nuclear accident. *Energy Environ. Sci.* **2012**, *5*, 8743–8757. [[CrossRef](#)]
3. Zhang, X.; da Silva, I.; Godfrey, H.G.W.; Callear, S.K.; Sapchenko, S.A.; Cheng, Y.; Vitorica-Yrezabal, I.; Frogley, M.D.; Cinque, G.; Tang, C.C.; et al. Confinement of Iodine Molecules into Triple-Helical Chains within Robust Metal-Organic Frameworks. *J. Am. Chem. Soc.* **2017**, *139*, 16289–16296. [[CrossRef](#)] [[PubMed](#)]

4. Kupper, F.C.; Feiters, M.C.; Olofsson, B.; Kaiho, T.; Yanagida, S.; Zimmermann, M.B.; Carpenter, L.J.; Luther, G.W., 3rd; Lu, Z.; Jonsson, M.; et al. Commemorating two centuries of iodine research: An interdisciplinary overview of current research. *Angew. Chem. Int. Ed.* **2011**, *50*, 11598–11620. [[CrossRef](#)] [[PubMed](#)]
5. Sava, D.F.; Rodriguez, M.A.; Chapman, K.W.; Chupas, P.J.; Greathouse, J.A.; Crozier, P.S.; Nenoff, T.M. Capture of volatile iodine, a gaseous fission product, by zeolitic imidazolate framework-8. *J. Am. Chem. Soc.* **2011**, *133*, 12398–12401. [[CrossRef](#)]
6. Ewing, R.C.; von Hippel, F.N. Nuclear Waste Management in the United States-Starting Over. *Science* **2009**, *325*, 151–152. [[CrossRef](#)]
7. Koenig, T.K.; Baidar, S.; Campuzano-Jost, P.; Cuevas, C.A.; Dix, B.; Fernandez, R.P.; Guo, H.; Hall, S.R.; Kinnison, D.; Nault, B.A.; et al. Quantitative detection of iodine in the stratosphere. *Proc. Natl. Acad. Sci. USA* **2020**, *117*, 1860–1866. [[CrossRef](#)]
8. Feng, Y.; Yang, P.; Li, Y.; Gu, J. AgNPs-Containing Metal–Organic Frameworks for the Effective Adsorption and Immobilization of Radioactive Iodine. *J. Chem. Eng. Data* **2020**, *65*, 1986–1992. [[CrossRef](#)]
9. Lin, G.; Zhu, L.; Duan, T.; Zhang, L.; Liu, B.; Lei, J. Efficient capture of iodine by a polysulfide-inserted inorganic NiTi-layered double hydroxides. *Chem. Eng. J.* **2019**, *378*, 1986–1992. [[CrossRef](#)]
10. Wang, X.B.; Yu, C.; Guo, H.; Cheng, Y.Q.; Li, Y.W.; Zheng, D.Y.; Feng, S.S.; Lin, Y.X. Robust fluorescent detection of iodine vapor by a film sensor based on a polymer of intrinsic microporosity. *Chem. Eng. J.* **2022**, *438*, 8. [[CrossRef](#)]
11. Zhou, W.; Yu, C.; Wang, X. Fast and Quantitative Electrical Detection of Iodine Based on a Polymer of Intrinsic Microporosity. *ACS Appl. Polym. Mater.* **2022**, *4*, 9151–9159. [[CrossRef](#)]
12. Diaz-Ramirez, M.L.; Vargas, B.; Raziell Alvarez, J.; Landeros-Rivera, B.; Rivera-Almazo, M.; Ramos, C.; Gabriel Flores, J.; Morales, E.; Vargas, R.; Garza, J.; et al. Fluorometric detection of iodine by MIL-53(Al)-TDC. *Dalton Trans.* **2020**, *49*, 6572–6577. [[CrossRef](#)] [[PubMed](#)]
13. Small, L.J.; Hill, R.C.; Krumhansl, J.L.; Schindelholz, M.E.; Chen, Z.; Chapman, K.W.; Zhang, X.; Yang, S.; Schroder, M.; Nenoff, T.M. Reversible MOF-Based Sensors for the Electrical Detection of Iodine Gas. *ACS Appl. Mater. Interfaces* **2019**, *11*, 27982–27988. [[CrossRef](#)] [[PubMed](#)]
14. Small, L.J.; Nenoff, T.M. Direct Electrical Detection of Iodine Gas by a Novel Metal–Organic–Framework–Based Sensor. *ACS Appl. Mater. Interfaces* **2017**, *9*, 44649–44655. [[CrossRef](#)] [[PubMed](#)]
15. Tan, J.; Namuangruk, S.; Kong, W.; Kungwan, N.; Guo, J.; Wang, C. Manipulation of Amorphous-to-Crystalline Transformation: Towards the Construction of Covalent Organic Framework Hybrid Microspheres with NIR Photothermal Conversion Ability. *Angew. Chem. Int. Ed.* **2016**, *55*, 13979–13984. [[CrossRef](#)]
16. Uribe-Romo, F.J.; Hunt, J.R.; Furukawa, H.; Klock, C.; O’Keeffe, M.; Yaghi, O.M. A Crystalline Imine-Linked 3-D Porous Covalent Organic Framework. *J. Am. Chem. Soc.* **2009**, *131*, 4570–4571. [[CrossRef](#)] [[PubMed](#)]
17. Kandambeth, S.; Mallick, A.; Lukose, B.; Mane, M.V.; Heine, T.; Banerjee, R. Construction of crystalline 2D covalent organic frameworks with remarkable chemical (acid/base) stability via a combined reversible and irreversible route. *J. Am. Chem. Soc.* **2012**, *134*, 19524–19527. [[CrossRef](#)] [[PubMed](#)]
18. Ding, S.-Y.; Gao, J.; Wang, Q.; Zhang, Y.; Song, W.-G.; Su, C.-Y.; Wang, W. Construction of Covalent Organic Framework for Catalysis: Pd/COF-LZU1 in Suzuki–Miyaura Coupling Reaction. *J. Am. Chem. Soc.* **2011**, *133*, 19816–19822. [[CrossRef](#)]
19. Xu, H.; Gao, J.; Jiang, D. Stable, crystalline, porous, covalent organic frameworks as a platform for chiral organocatalysts. *Nat. Chem.* **2015**, *7*, 905–912. [[CrossRef](#)] [[PubMed](#)]
20. Wang, X.; Han, X.; Zhang, J.; Wu, X.; Liu, Y.; Cui, Y. Homochiral 2D Porous Covalent Organic Frameworks for Heterogeneous Asymmetric Catalysis. *J. Am. Chem. Soc.* **2016**, *138*, 12332–12335. [[CrossRef](#)]
21. de Combarieu, G.; Morcrette, M.; Millange, E.; Guillou, N.; Cabana, J.; Grey, C.P.; Margiolaki, I.; Férey, G.; Tarascon, J.M. Influence of the Benzoquinone Sorption on the Structure and Electrochemical Performance of the MIL-53(Fe) Hybrid Porous Material in a Lithium-Ion Battery. *Chem. Mater.* **2009**, *21*, 1602–1611. [[CrossRef](#)]
22. Chmiola, J.; Yushin, G.; Gogotsi, Y.; Portet, C.; Simon, P.; Taberna, P.L. Anomalous Increase in Carbon Capacitance at Pore Sizes Less Than 1 Nanometer. *Science* **2006**, *313*, 1760–1763. [[CrossRef](#)]
23. Chandra, S.; Kundu, T.; Kandambeth, S.; BabaRao, R.; Marathe, Y.; Kunjir, S.M.; Banerjee, R. Phosphoric Acid Loaded Azo (–N=N–) Based Covalent Organic Framework for Proton Conduction. *J. Am. Chem. Soc.* **2014**, *136*, 6570–6573. [[CrossRef](#)]
24. Ding, S.-Y.; Dong, M.; Wang, Y.-W.; Chen, Y.-T.; Wang, H.-Z.; Su, C.-Y.; Wang, W. Thioether-Based Fluorescent Covalent Organic Framework for Selective Detection and Facile Removal of Mercury(II). *J. Am. Chem. Soc.* **2016**, *138*, 3031–3037. [[CrossRef](#)]
25. Yuan, H.; Li, N.; Linghu, J.; Dong, J.; Wang, Y.; Karmakar, A.; Yuan, J.; Li, M.; Buenconsejo, P.J.S.; Liu, G.; et al. Chip-Level Integration of Covalent Organic Frameworks for Trace Benzene Sensing. *ACS Sens.* **2020**, *5*, 1474–1481. [[CrossRef](#)]
26. Yuan, S.S.; Li, X.; Zhu, J.Y.; Zhang, G.; Van Puyvelde, P.; Van der Bruggen, B. Covalent organic frameworks for membrane separation. *Chem. Soc. Rev.* **2019**, *48*, 2665–2681. [[CrossRef](#)] [[PubMed](#)]
27. Zhao, Y.X.; Liu, X.; Li, Y.P.; Xia, M.; Xia, T.; Sun, H.C.; Sui, Z.Y.; Hu, X.M.; Chen, Q. Ultra-stable fluorescent 2D covalent organic framework for rapid adsorption and selective detection of radioiodine. *Microporous Mesoporous Mater.* **2021**, *319*, 6. [[CrossRef](#)]
28. Chang, J.; Li, H.; Zhao, J.; Guan, X.; Li, C.; Yu, G.; Valtchev, V.; Yan, Y.; Qiu, S.; Fang, Q. Tetrathiafulvalene-based covalent organic frameworks for ultrahigh iodine capture. *Chem. Sci.* **2021**, *12*, 8452–8457. [[CrossRef](#)] [[PubMed](#)]
29. Xie, Y.; Pan, T.; Lei, Q.; Chen, C.; Dong, X.; Yuan, Y.; Maksoud, W.A.; Zhao, L.; Cavallo, L.; Pinnau, I.; et al. Efficient and simultaneous capture of iodine and methyl iodide achieved by a covalent organic framework. *Nat. Commun.* **2022**, *13*, 2878. [[CrossRef](#)] [[PubMed](#)]

30. Gao, Q.; Li, X.; Ning, G.H.; Leng, K.; Tian, B.B.; Liu, C.B.; Tang, W.; Xu, H.S.; Loh, K.P. Highly photoluminescent two-dimensional imine-based covalent organic frameworks for chemical sensing. *Chem. Commun.* **2018**, *54*, 2349–2352. [[CrossRef](#)] [[PubMed](#)]
31. Zhang, S.J.; Liu, D.Q.; Wang, G.T. Covalent Organic Frameworks for Chemical and Biological Sensing. *Molecules* **2022**, *27*, 2586. [[CrossRef](#)]
32. Chen, S.D.; Yuan, B.Q.; Liu, G.; Zhang, D.J. Electrochemical Sensors Based on Covalent Organic Frameworks: A Critical Review. *Front. Chem.* **2020**, *8*, 11. [[CrossRef](#)] [[PubMed](#)]
33. Li, Q.; Lan, X.; An, G.; Ricardez-Sandoval, L.; Wang, Z.; Bai, G. Visible-Light-Responsive Anthraquinone Functionalized Covalent Organic Frameworks for Metal-Free Selective Oxidation of Sulfides: Effects of Morphology and Structure. *ACS Catal.* **2020**, *10*, 6664–6675. [[CrossRef](#)]
34. Geng, Q.; Wang, H.; Wu, Y.; Lv, L.P.; Chen, S.; Sun, W.; Wang, Y. Covalent-Induced Heterostructure of Covalent-Organic Frameworks and MXene as Advanced Electrodes with Motivated Pseudocapacitance Performance. *ChemElectroChem* **2022**, *9*, 9. [[CrossRef](#)]
35. DeBlase, C.R.; Silberstein, K.E.; Truong, T.T.; Abruna, H.D.; Dichtel, W.R. beta-Ketoenamine-linked covalent organic frameworks capable of pseudocapacitive energy storage. *J. Am. Chem. Soc.* **2013**, *135*, 16821–16824. [[CrossRef](#)]
36. Wu, Y.; Yan, D.; Zhang, Z.; Matsushita, M.M.; Awaga, K. Electron Highways into Nanochannels of Covalent Organic Frameworks for High Electrical Conductivity and Energy Storage. *ACS Appl. Mater. Interfaces* **2019**, *11*, 7661–7665. [[CrossRef](#)]
37. Dong, X.; He, Q.; Li, M.; Wang, X.; Wang, Y.; Zhang, W. Fluorescence and electrochemical detection of iodine vapor in the presence of high humidity using Ln-based MOFs. *Dalton Trans.* **2021**, *50*, 15567–15575. [[CrossRef](#)]
38. Zhu, H.; Geng, T.M.; Tang, K.B. The cyclotriphosphazene-based covalent organic frameworks constructed entirely by flexible building blocks for adsorbing and fluorescence sensing iodine. *Microporous Mesoporous Mater.* **2022**, *343*, 10. [[CrossRef](#)]
39. Zhai, L.P.; Han, D.D.; Dong, J.H.; Jiang, W.Q.; Nie, R.M.; Yang, X.B.; Luo, X.L.; Li, Z.P. Constructing Stable and Porous Covalent Organic Frameworks for Efficient Iodine Vapor Capture. *Macromol. Rapid Commun.* **2021**, *42*, 7. [[CrossRef](#)]
40. Wu, Z.N.; Wei, W.; Ma, J.G.; Luo, J.Q.; Zhou, Y.M.; Zhou, Z.Y.; Liu, S.J. Adsorption of Iodine on Adamantane-Based Covalent Organic Frameworks. *ChemistrySelect* **2021**, *6*, 10141–10148. [[CrossRef](#)]
41. Yang, Y.-X.; Tang, X.-H.; Wu, J.-L.; Dong, Z.-Y.; Yan, Y.-L.; Zheng, S.-R.; Fan, J.; Li, X.; Cai, S.; Zhang, W.-G. Transformation of a Hydrazone-Linked Covalent Organic Framework into a Highly Stable Hydrazide-Linked One. *ACS Appl. Polym. Mater.* **2022**, *4*, 4624–4631. [[CrossRef](#)]
42. Zhang, Z.; Dong, X.; Yin, J.; Li, Z.G.; Li, X.; Zhang, D.; Pan, T.; Lei, Q.; Liu, X.; Xie, Y.; et al. Chemically Stable Guanidinium Covalent Organic Framework for the Efficient Capture of Low-Concentration Iodine at High Temperatures. *J. Am. Chem. Soc.* **2022**, *144*, 6821–6829. [[CrossRef](#)] [[PubMed](#)]
43. Holzapfel, M.; Martinent, A.; Alloin, F.; Le Gorrec, B.; Yazami, R.; Montella, C. First lithiation and charge/discharge cycles of graphite materials, investigated by electrochemical impedance spectroscopy. *J. Electr. Chem.* **2003**, *546*, 41–50. [[CrossRef](#)]
44. Zhang, R.; Lu, L.H.; Chang, Y.Y.; Liu, M. Gas sensing based on metal-organic frameworks: Concepts, functions, and developments. *J. Hazard. Mater.* **2022**, *429*, 27. [[CrossRef](#)] [[PubMed](#)]

Disclaimer/Publisher's Note: The statements, opinions and data contained in all publications are solely those of the individual author(s) and contributor(s) and not of MDPI and/or the editor(s). MDPI and/or the editor(s) disclaim responsibility for any injury to people or property resulting from any ideas, methods, instructions or products referred to in the content.